Supporting Information

Interface engineering of Co_2B-MoO_3/MOF heterojunction with rich cobalt defects for highly enhanced $NaBH_4$ hydrolysis

Chenxi Shang [a], Luyan Shi [a], Shuqing Zhou [a], Sheraz Muhammad [a], Tayirjan Taylor Isimjan [b, *], Huancheng Hu [a, *], Xiulin Yang [a, *]

[a] *Guangxi Key Laboratory of Low Carbon Energy Materials, School of Chemistry and Pharmaceutical Sciences, Guangxi Normal University, Guilin 541004, China*

[b] *Saudi Arabia Basic Industries Corporation (SABIC) at King Abdullah University of Science and Technology (KAUST), Thuwal 23955-6900, Saudi Arabia*

** Corresponding author.*

E-mail address: xlyang@gxnu.edu.cn (X. Yang), isimjant@sabic.com (T.T. Isimjan), siniantongnian@126.com (H. Hu)

1. Experimental section

Materials

Cobalt nitrate hexahydrate ($Co(NO_3)_2·6H_2O$, ≥ 99.0%, Aladdin), cobalt chloride hexahydrate ($CoCl_2·6H_2O$, ≥ 99.0%, Aladdin), sodium borohydride ($NaBH_4$, ≥ 98.0%, Sinopharm Group), sodium hydroxide (NaOH, ≥ 96.0%, Aladdin), urea (H_2NCONH_2, ≥ 99.0%, Aladdin), ethanol (C_2H_6O, ≥ 99.7%, Xilong Scientific), sodium molybdate dihydrate ($Na_2MoO_4·2H_2O$, ≥ 99.0%, Xilong Scientific), ammonium acetate (CH_3COONH_4, ≥ 98.0%, Xilong Scientific), N,N-Dimethylformamide (DMF) and Trimesic acid-1,3,5-Benzenetricarboxylic acid ($C_9H_6O_6$ (H_3BTC), ≥ 98%, Aladdin). All reagents were commercially available and could be used directly without further purification. All aqueous solutions were prepared with deionized water.

Synthesis of Co-BTC (MOF)

This study synthesized Co-BTC using the conventional method, as previously reported in the literature.[1] Initially, 2 mmol $Co(NO_3)_2·6H_2O$ and 0.7 mmol trimesic acid were mixed in 10 mL of DMF and stirred for 10 min. Subsequently, 5 mL of 1 M ammonium acetate solution was added, stirring the mixture for 30 min. The mixture was then transferred to a 20 mL Teflon-lined autoclave and maintained at 150 °C for 24 h. After cooling to room temperature and being washed thrice with DMF, the product was centrifuged and dried in a 60 °C oven overnight to produce Co-BTC (In the subsequent synthetic sections of this article, when Co-BTC serves as a carrier, we represent it with MOF).

Synthesis of Co_2B-MoO_3/MOF

Co_2B-MoO_3/MOF heterojunction materials were prepared using incipient wet impregnation and $NaBH_4$ reduction methods. First, 30 mg of MOF was dispersed in 10 mL of ethanol by sonication. Then, $CoCl_2 \cdot 6H_2O$ and $Na_2MoO_4 \cdot 2H_2O$ were added into the suspension and stirred for 1 h. The solvent was then evaporated under a vacuum, obtaining Co^{2+}/Mo^{6+}-MOF. The Co^{2+}/Mo^{6+}-MOF was mixed with 0.8 g urea in a mortar and ground manually. Next, 4 mmol of $NaBH_4$ was added and uniformly dispersed into the mortar, grinding by hand until the mixture turned black. The mixture was then transferred to a glass vessel, and an appropriate amount of deionized water was added. The obtained samples were centrifuged, washed three times with water and alcohol, and vacuum-dried at 60 °C for 12 h. For comparison, while maintaining the total mass of the metal salt at 0.14 g, other Co_2B-MoO_3/MOF composites were prepared by varying the Co/Mo molar ratio (1:1, 4:1, 6:1, 13:1, 20:1) during the synthesis process. The MoB/MOF and Co_2B-Co/MOF were prepared using the same method without adding $CoCl_2 \cdot 6H_2O$ or $Na_2MoO_4 \cdot 2H_2O$. Similarly, Co_2B was synthesized through the same procedure, excluding $Na_2MoO_4 \cdot 2H_2O$ and MOF.

2. Physical characterization

The structural integrity of samples was analyzed by X-ray diffraction (XRD, Rigaku 13 D/Max 2500 V/PC, Japan). The specific surface and pore size distribution of catalysts were calculated by Brunauer-Emmett-Teller (BET) and the Barrett-Joyner-Halenda (BJH) methods, respectively. The surface valence of material was analyzed by X-ray photoelectron spectroscopy (XPS, JPS-9010 Mg Kα). Zeta potential was determined on a Litesizer 500. The field-emission scanning electron microscopy (SEM, FEI Quanta 200 FEG) and transmission electron microscopy (TEM, JEM-2100F) were used to characterize the morphology and

microstructure of samples. The water contact angle was investigated using an optical contact angle meter (Dataphysics-OCA20). Electron paramagnetic resonance (EPR) spectra were measured by Bruker E500 spectrometer. Metal contents were investigated by inductively coupled plasma mass spectroscopy (ICP-MS, PekinElmer corporation, FLexar-NexION300X). The work function (WF) was acquired by ultraviolet photoelectron spectroscopy (UPS). Using a He (I) discharge lamp emitting the He photoelectron line (21.22 eV), the cutoff energy (E_{cutoff}), valence band maximum (E_v), and Fermi level (E_f) were extracted from the UPS spectra. The Ag layer acted as a reference to measure the kinetic energy corresponding to the E_f and then the E_f was corrected to 0 eV.

The WF was calculated according to equation.[2] : $WF = 21.22 - E_{cutoff}$

3. Catalytic measurements

The catalytic activity, reusability, and activation energy of the catalytic materials were determined using the following test methods. Typically, a 25 mL mixture solution (containing 150 mM $NaBH_4$ + 0.4 wt.% NaOH) was kept in a three-necked round-bottom flask (50 mL), and maintained it in a water bath at 25 °C. The volume of H_2 is monitored by a computer-connected drainage system, which records instantaneous changes in water volume. The catalytic reaction was started when the catalyst was added to the flask under constant magnetic stirring conditions. Five consecutive cycling tests were conducted at 25 °C to assess the reusability of the catalyst. We used fresh $NaBH_4$ solution instead of fully decomposed $NaBH_4$. After each reusability test, we centrifuged the catalytic material, washed it several times using deionized water and anhydrous ethanol, dried it under vacuum at room temperature, and weighed the catalytic material for the next cycle experiment. All

performance tests were performed three times under the same conditions, and the experimental results were averaged to ensure accuracy. The activation energy of the designed catalysts was evaluated in the temperature range of 25 ~ 45 °C using the same apparatus.

4. Calculation of catalytic performance

(1) The hydrogen production rate of the catalyst at different temperatures was analyzed by applying the Arrhenius equation and the following equation was derived:

$$\ln \kappa = \ln A - E_a/RT \quad (1)$$

Where κ (L min^{-1} g^{-1}) is the rate coefficient, A (L min^{-1} g^{-1}) is a constant, E_a (kJ mol^{-1}) is the activation energy, R (8.314 J mol^{-1} K^{-1}) is the universal gas constant, and T (K) is testing temperature.

(2) The specific H_2 generation rate (HGR) is calculated as follows:

$$HGR = \frac{V_{H_2O}\,(mL)}{t\,(min) \times m\,(g)} \quad (2)$$

Where V_{H_2O} denotes the drainage volume, m refers to the catalyst mass, and t is the reaction time.

5. Supplementary Figures and Table

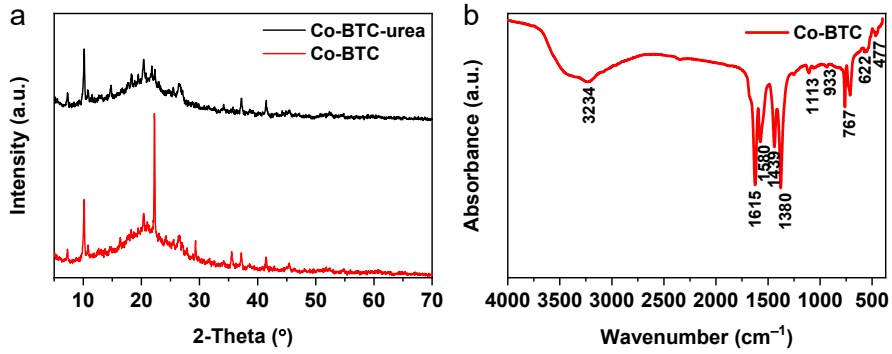

Fig. S1. (a) XRD patterns of Co-BTC-urea. (b) FT-IR spectra of Co-BTC.

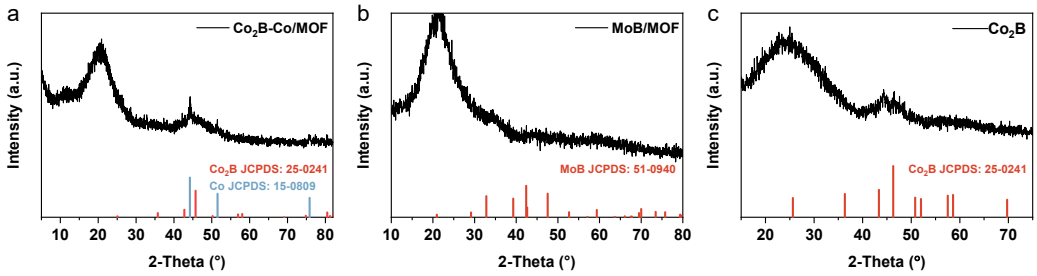

Fig. S2. XRD patterns of (a) Co_2B-Co/MOF, (b) MoB/MOF, and (c) Co_2B.

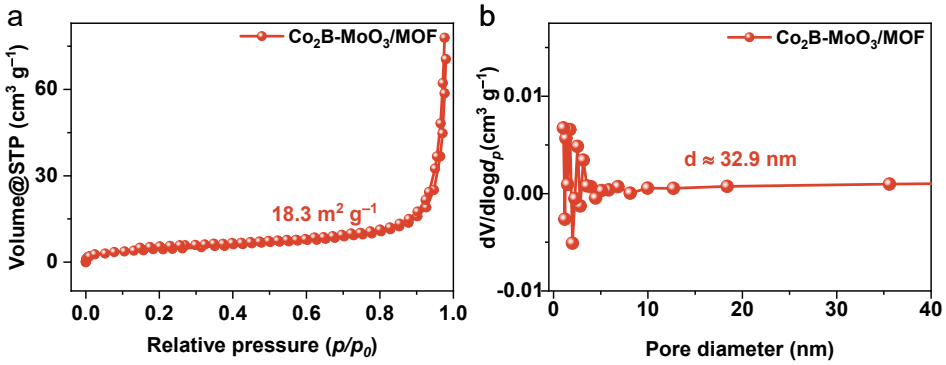

Fig. S3. (a) N_2 adsorption/desorption isotherm and (b) the corresponding pore size distribution of Co_2B-MoO_3/MOF.

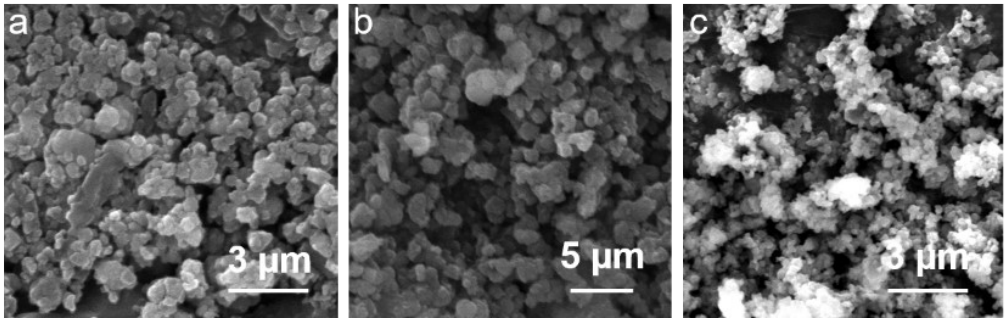

Fig. S4. SEM images of (a) Co-BTC, (b) Co_2B-Co/MOF, and (c) Co_2B.

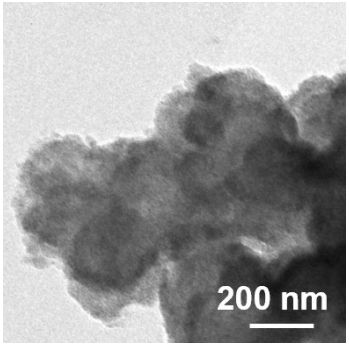

Fig. S5. TEM image of Co_2B-Co/MOF.

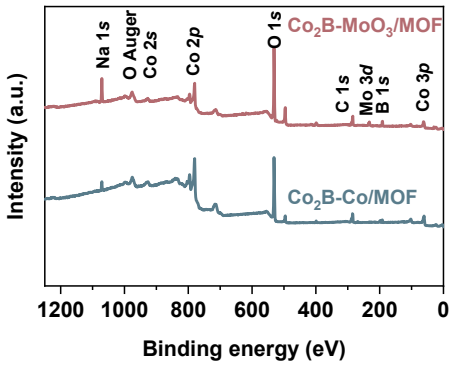

Fig. S6. XPS survey spectra of Co_2B-MoO_3/MOF and Co_2B-Co/MOF.

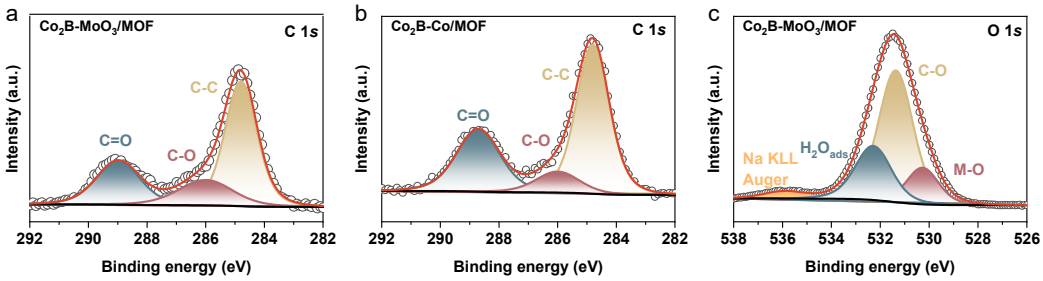

Fig. S7. High-resolution XPS spectra of C 1*s* of (a) Co_2B-MoO_3/MOF and (b) Co_2B-Co/MOF. (c) O 1*s* for Co_2B-MoO_3/MOF.

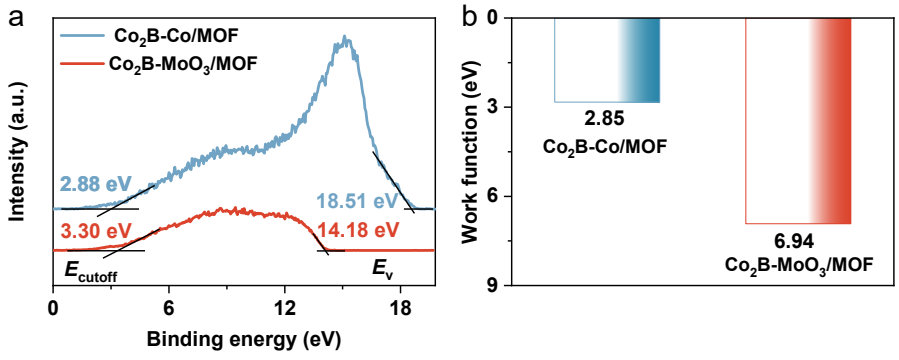

Fig. S8. (a) UPS spectra and (b) work functions of the different catalysts.

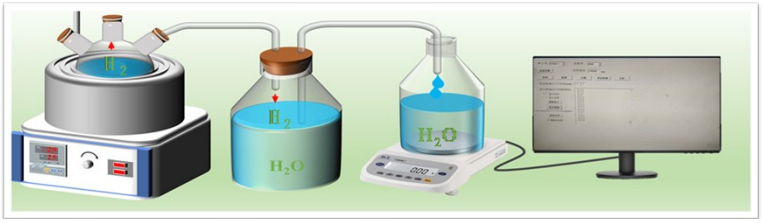

Fig. S9. Schematic diagram of the setup for H_2 production by hydrolysis of 150 mM $NaBH_4$ + 0.4 wt.% NaOH solution.

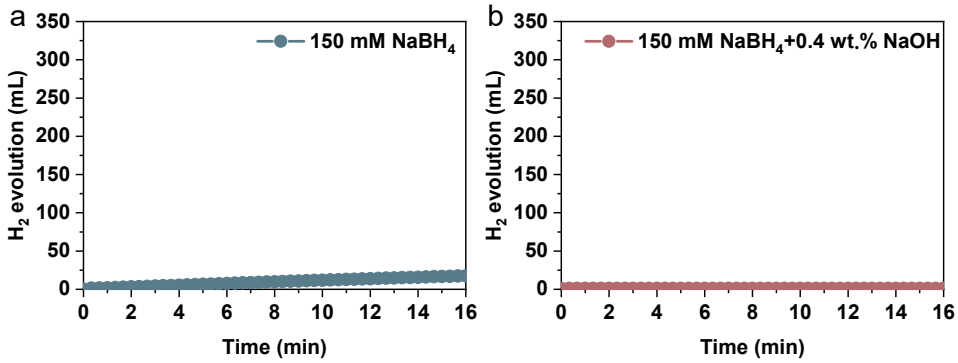

Fig. S10. (a) Self-hydrolysis of $NaBH_4$ study of 150 mM $NaBH_4$ solution at 25 ºC. (b) Self-hydrolysis of $NaBH_4$ study of 150 mM $NaBH_4$ + 0.4 wt.% NaOH solution at 25 ºC.

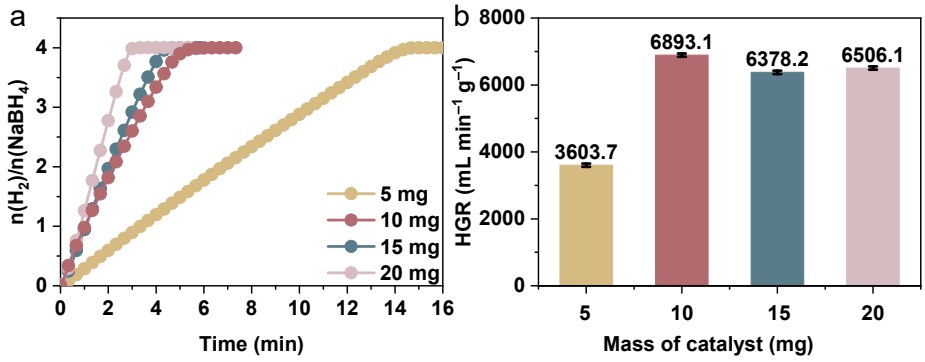

Fig. S11. (a) The equivalent H_2 per mole of sodium borohydride versus time with different mass of catalyst and (b) the corresponding HGR values. All tests were performed at 298 K.

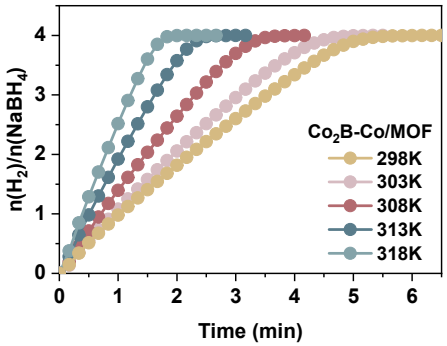

Fig. S12. The relationship between the H_2 generation rate and applied temperatures of Co_2B-Co/MOF for alkalized $NaBH_4$ hydrolysis.

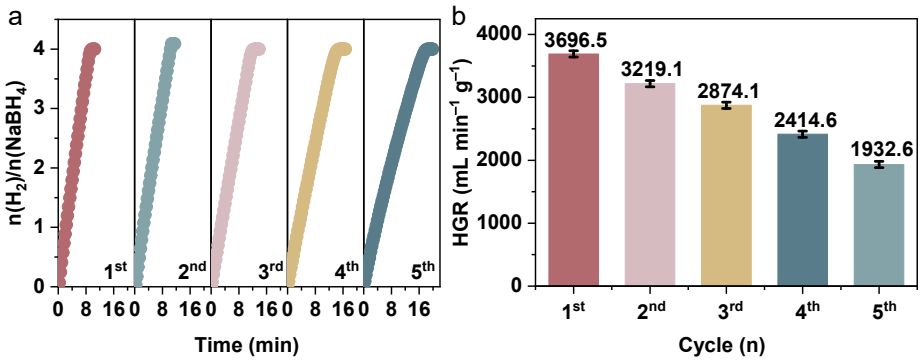

Fig. S13. (a) Reusability test of Co_2B-Co/MOF catalyst in alkaline $NaBH_4$ solution at 25 °C and (b) the corresponding HGR values in the different cycle.

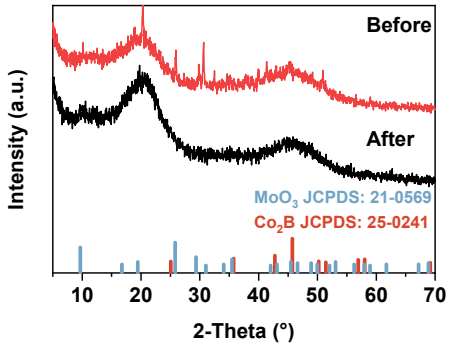

Fig. S14. XRD patterns before and after catalyzing the hydrolysis of $NaBH_4$ for 5 times in 150 mM $NaBH_4$ + 0.4 wt.% NaOH solution.

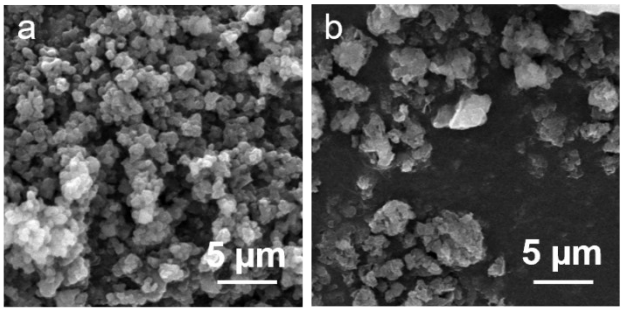

Fig. S15. SEM images of Co_2B-MoO_3/MOF (a) before and (b) after catalyzing the hydrolysis of $NaBH_4$ for 5 times in 150 mM $NaBH_4$ + 0.4 wt.% NaOH solution.

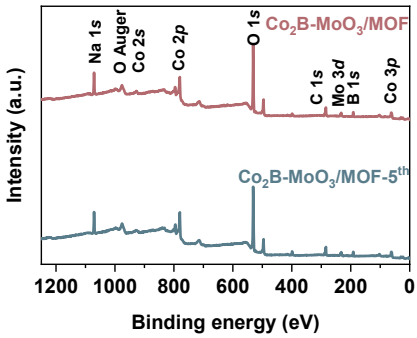

Fig. S16. XPS survey spectra of Co_2B-MoO_3/MOF and Co_2B-MoO_3/MOF catalyst after 5 test cycles.

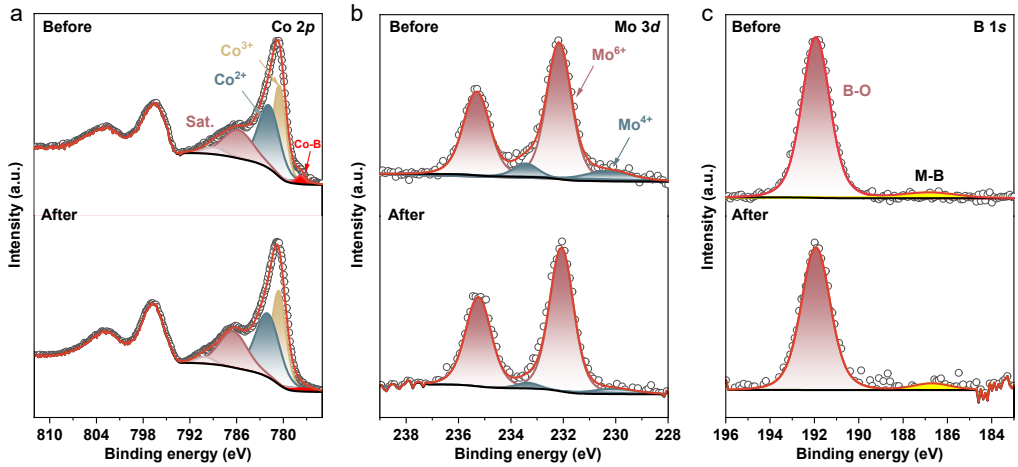

Fig. S17. Comparison of the high-resolution (a) Co 2*p*, (b) Mo 3*d*, (c)B 1*s* XPS spectrum of Co_2B-MoO_3/MOF catalysts after cycling for 5 times.

Table S1. Inductive coupled plasma mass spectroscopy (ICP-MS) results of Co_2B-MoO_3/MOF.

Catalysts	Co (wt. %)	Mo (wt. %)	Molar ratio of Co/Mo
Co_2B-MoO_3/MOF	51.3	3.6	14.3/1
Co_2B-MoO_3/MOF-5th	82.6	4.2	19.6/1

Note: The catalyst sample of 2.0 mg was weighed and dissolved in 8 mL aqua regia solution, followed by taking 80 μL solution to 100 mL volumetric flask with a pipette and diluted to 200 μg L^{-1} before ICP testing. The standard solution of Co and Mo was purchased from commercial company and used directly.

Table S2. The summarized various parameters of catalysts that facilitate the production of H_2 through hydrolysis of $NaBH_4$.

Catalysts	Specific rate (mL min^{-1} g_{cat}^{-1})	Activation energy (kJ mol^{-1})	Solute	Temperature (°C)
Co_2B-MoO_3/MOF	**6893.1**	**50.5**	**150 mM $NaBH_4$ + 0.4 wt.% NaOH**	**25**
Co/$CuFe_2O_4$ [3]	2937	18.2	2 wt.% $NaBH_4$ + 4 wt.% NaOH	35
Co@NHC [4]	1515.4	12.6	0.125 M $NaBH_4$ + 0.8 wt.% NaOH	25
Co_2B-Fe_2B [5]	5316	33.4	150 mM $NaBH_4$ + 0.4 wt.% NaOH	25
UiO-66 [6]	6200	N.A	0.05 M $NaBH_4$	30
Ru/ZIF-67 [7]	5520	N.A.	4.7 mg/mL $NaBH_4$	30
CoWB/NF [8]	14130	18.15	5 wt.% $NaBH_4$ + 2 wt.% NaOH	30
Co/Fe-BDC MOFs [9]	1159	N.A.	40 mg $NaBH_4$ + 10 mg NaOH	25
CoB [10]	1486	21.4	5 wt.% $NaBH_4$ + 1 wt.% NaOH	30
Co-Ce-B [11]	4760	33.1	1.5 wt.% $NaBH_4$ + 5 wt.% NaOH	30
Co@NMGC [12]	3775	35.2	1.5 wt.% $NaBH_4$ + 1 wt.% NaOH	25±0.1
Ru-Fe/GO [13]	473	59.33	10 wt.% $NaBH_4$ + 1 wt.% NaOH	25
CoP nanosheet [14]	6100	41	1 wt.% $NaBH_4$ + 2 wt.% NaOH	25
Ni/Au/Co [15]	N.A.	53.4	30 mM $NaBH_4$, pH=12	20±0.5
Fe-CoP/Ti [16]	6060	47.8	1 wt.% $NaBH_4$ + 1 wt.% NaOH	25
Co-Cu-B [17]	2120	30	2.5 wt.% $NaBH_4$ + 5 wt.% NaOH	25
RuO_2-CoP [18]	10713	43.3	6 wt.% $NaBH_4$ + 4 wt.% NaOH	30
Co-B-P [19]	3976	30.84	2.5 wt.% $NaBH_4$ + 5 wt.% NaOH	30

References

1. Z. Haiyang, L. Jie, L. Zhiqiang, S. Yayun, Z. Siyan, W. Junchuan, S. Ying, Z. Xueqin and L. Baoping, Influence of Co-MOF morphological modulation on its electrochemical performance, *J. Phys. Chem. Solids*, 2022, **160**, 110336.
2. D. Chen, R. Lu, R. Yu, Y. Dai, H. Zhao, D. Wu, P. Wang, J. Zhu, Z. Pu, L. Chen, J. Yu and S. Mu, Work-function-induced Interfacial Built-in Electric Fields in Os-$OsSe_2$ Heterostructures for Active Acidic and Alkaline Hydrogen Evolution, *Angew. Chem. Int.*

Ed., 2022, **61**, e202208642.

3. F. Mirshafiee and M. Rezaei, Enhancing hydrogen generation from sodium borohydride hydrolysis and the role of a Co/$CuFe_2O_4$ nanocatalyst in a continuous flow system, *Sci. Rep*, 2024, **14**, 9659.
4. D. T. Tran, H. T. Van, L. H. Nguyen, N. Van Quang, Y.-c. Tsai, K.-Y. A. Lin and D. D. Tuan, Hierarchical porous cobalt nanoparticles encapsulated in heteroatom-doped hollow carbon as an enhancing multifunctional catalyst for hydrolysis of sodium borohydride and hydrogenation of bromate in water, *Surf. Interfaces*, 2024, **48**, 104329.
5. S. Zhou, L. Cheng, Y. Liu, J. Tian, C. Niu, W. Li, S. Xu, T. T. Isimjan and X. Yang, Highly active and robust catalyst: Co_2B-Fe_2B heterostructural nanosheets with abundant defects for hydrogen production, *Inorg. Chem*, 2024, **63**, 2015-2023.
6. H. N. Abdelhamid, UiO-66 as a catalyst for hydrogen production via the hydrolysis of sodium borohydride, *Dalton Trans.*, 2020, **49**, 10851-10857.
7. D. D. Tuan and K.-Y. A. Lin, Ruthenium supported on ZIF-67 as an enhanced catalyst for hydrogen generation from hydrolysis of sodium borohydride, *Chem. Eng. J.*, 2018, **351**, 48-55.
8. Y. Wei, M. Wang, W. Fu, L. Wei, X. Zhao, X. Zhou, M. Ni and H. Wang, Highly active and durable catalyst for hydrogen generation by the $NaBH_4$ hydrolysis reaction: CoWB/NF nanodendrite with an acicular array structure, *J. Alloys Compd.*, 2020, **836**, 155429.
9. M. Alaide de Oliveira, E. Silva Souza, J. de Jesus Santana, N. Łukasik, B. Stefany Lima da Silva, B. Silva Barros and J. Kulesza, M-BDC (M = Co and/ or Fe) MOFs as effective catalysts for hydrogen generation via hydrolysis of sodium borohydride, *Appl. Surf. Sci.*, 2023, **628**, 157361.
10. N. Selvitepe, A. Balbay and C. Saka, Optimisation of sepiolite clay with phosphoric acid treatment as support material for CoB catalyst and application to produce hydrogen from the $NaBH_4$ hydrolysis, *Int. J. Hydrogen Energy*, 2019, **44**, 16387-16399.
11. Y. Zou, Y. Yin, Y. Gao, C. Xiang, H. Chu, S. Qiu, E. Yan, F. Xu and L. Sun, Chitosan-mediated Co-Ce-B nanoparticles for catalyzing the hydrolysis of sodium borohydride, *Int. J. Hydrogen Energy*, 2018, **43**, 4912-4921.

12. J. Li, X. Hong, Y. Wang, Y. Luo, P. Huang, B. Li, K. Zhang, Y. Zou, L. Sun, F. Xu, F. Rosei, S. P. Verevkin and A. A. Pimerzin, Encapsulated cobalt nanoparticles as a recoverable catalyst for the hydrolysis of sodium borohydride, *Energy Stor. Mater*, 2020, **27**, 187-197.
13. Y. Zhang, J. Zou, Y. Luo and F. Wang, Study on preparation and performance of Ru-Fe/GO catalyst for sodium borohydride alcoholysis to produce hydrogen, *Fullerenes, Nanotubes Carbon Nanostruct.*, 2020, **28**, 786-793.
14. T. Liu, K. Wang, G. Du, A. M. Asiri and X. Sun, Self-supported CoP nanosheet arrays: a non-precious metal catalyst for efficient hydrogen generation from alkaline $NaBH_4$ solution, *J. Mater. Chem. A*, 2016, **4**, 13053-13057.
15. C. Jiao, Z. Huang, X. Wang, H. Zhang, L. Lu and S. Zhang, Synthesis of Ni/Au/Co trimetallic nanoparticles and their catalytic activity for hydrogen generation from alkaline sodium borohydride aqueous solution, *RSC Adv.*, 2015, **5**, 34364-34371.
16. C. Tang, R. Zhang, W. Lu, L. He, X. Jiang, A. M. Asiri and X. Sun, Fe-doped CoP nanoarray: a monolithic multifunctional catalyst for highly efficient hydrogen generation, *Adv. Mater.*, 2017, **29**, 1602441.
17. M. S. İzgi, Ö. Şahin and C. Saka, Hydrogen production from $NaBH_4$ using Co-Cu-B catalysts prepared in methanol: Effect of plasma treatment, *Int. J. Hydrogen Energy*, 2016, **41**, 1600-1608.
18. S. Ye, Y. Wang, C. Wang, L. Cheng, L. Sun and P. Yan, Robust cellulose fiber/fibrous sepiolite coated RuO_2-CoP aerogel as monolithic catalyst for hydrogen generation via $NaBH_4$ hydrolysis, *J. Colloid Interface Sci.*, 2023, **639**, 284-291.
19. Ö. Şahin, D. E. Karakaş, M. Kaya and C. Saka, The effects of plasma treatment on electrochemical activity of Co-B-P catalyst for hydrogen production by hydrolysis of $NaBH_4$, *J. Energy Inst.*, 2017, **90**, 466-475.